Available online at www.garmian.edu.krd

Passer Journal

Passer 4 (Issue 2) (2022) 92-99

http://passer.garmian.edu.krd/

Investigation into Fiber Optic Seismic Sensor incorporating Fiber Bragg Grating Array

Riyam Alaa Johni[1*], Kanar Roshen Tariq[2], Roshen Tariq Ahmadhamdi[3], David Iyan Forsyth[4]

[1]*Kurdistan technical institute, Kurdistan Region, Iraq*
[2]*Technical College of Informatics, Sulaimani Polytechnic University, Sulaimaniyah, KRG, Iraq. Software Engineering, Qaiwan International University-UTM franchise, Sulaimaniyah, Kurdistan, Iraq.*
[3]*Energy and Renewable Energies Technology Center / University of Technology, Baghdad, Iraq.*
[4]*Electrical/Electronic computer engineering lecturer, HENAN POLYTECHNIC UNIVERSITY, No.2001, Shiji Road, Jiaozuo, Henan, PRC*

Received 08 February 2022; revised 25 June 2022;
accepted 26 June 2022; available online 17 July 2022

doi:10.24271/psr.46

ABSTRACT

This paper presents a theoretical study of various types of fiber optic sensing systems used for seismic monitoring integrating a series of fiber optic Bragg gratings (FBGs) into the sensor carrier. The interference network contains groups of interfering subnets, and each subnet contains multiple interference networks. Each interferometer in the subband is implemented with a specific pair of fiber Bragg gratings and the sensing length of the fiber is placed between each pair of fiber Bragg gratings. Each fiber Bragg grating pair has a similar characteristic wavelength modified from the characteristic wavelength of all other fiber Bragg grating pairs in the subband. The subarrays are interconnected to minimize crosstalk of common wavelengths between the sensors throughout the interferometer array. Our work is focused on investigating the selection of the best wavelength for use in the system. This study was performed using state-of-the-art simulation techniques for strain and temperature changes in FBG sensor arrays. The cumulative results obtained will help designers achieve optimized performance of similar fiber optic hydrophones in the future. The wavelength range of 1300 nm has been shown to provide the best performance for this type of fiber optic hydrophone system.

Keywords: Hydrophone, FBG sensor, wavelength, FBG array, sub-array, crosstalk, fiber optic sensing, seismic sensor.

1. Introduction

Technology in the telecommunications industry is ever-evolving, and the fiber optic sensor field has become one of the fastest growing technologies for specific applications[1]. One such example is the application of fiber optic hydrophones[2] to seismic sensors. This tool is beneficial for seismic exploration withinside the military, and oil, and fueloline industries, which particularly use sonar. One of the constraints of current sonar arrays primarily based totally on ceramic-electric powered sensors is they require a massive range of underwater electronics for facts multiplexing and telemetry[3].

This type of electronic device, combined with associated power supplies and telemetry cables, is very expensive, bulky, and can be prone to failure[4]. The consequences of water ingress due to sealing problems exacerbate reliability problems[5]. Some of these issues can be resolved by using new alternatives. For example, fiberglass hydrophones with Fiber Bragg Grating (FBG) are lightweight and less susceptible to electromagnetic fields[6]. Hydrophones can be used not only for communications such as data transmission, but also as sensors[7]. The most important parameters are temperature, hydrostatic pressure, and undersea stress[8]. A Fiber Bragg Grating (FBG) is an optical device obtained through introducing a modulation of the refractive index of the fiber core. Fiber Bragg grating (FBG) has wide attracted attention because of many of their inherent advantages such as cylindrical geometry, small size, light weight, environmentally robust compact size, high sensitivity, remote sensing capability, electromagnetic interference immunity, and radio frequency interface. This type of sensing system can be realized by using FBG network with special characteristics different from conventional fiber optic sensors. The FBG sensor has several advantages. Light weight, small size, low power consumption, etc. Many researchers have improved the existing fiber-optic hydrophone seismic sensors by incorporating FBGs[8,9].

* Corresponding author
E-mail address: ryam.johni@kti.edu.krd (MSc).
Peer-reviewed under the responsibility of the University of Garmian.

While regular fiber windows are recommended for most communication applications, research is being conducted on the optimal wavelength input for use with this type of fiber optic hydrophone sensor[10]. The common fiber windows used and recommended for the are 1300 nm and 1550 nm, the latter usually having the region with the lowest signal attenuation[11]. However, if fiber optic hydrophone systems are used for seismic acquisition to achieve optimum performance, it has been determined whether this is the same[12]. The combined results obtained may help designers optimize the performance of similar fiber optic hydrophones in the future. The wavelength range of 1300 nm has been shown to provide the best performance for this type of fiber optic underwater acoustic system. The fiber Bragg grating of each pair of fiber Bragg grating has the same characteristic wavelength, which is different from the characteristic wavelength of all other pairs of fiber Bragg grating in the grating. The subarrays are interconnected to decrease not unusual place wavelength crosstalk among the sensors withinside the not unusual place interferometer array. Our work is targeted on locating the best wavelength to apply withinside the system. This study was carried out using state-of-the-art methods to model stress and temperature changes in the FBG sensor network.

2. Fiber Optic Sensor Design

Fiber optic hydrophones were simulated using state-of-the-art simulation software Optisim[13]. Creating a system consists of three main parts which include transmitters, sensors and receivers as shows in figure (1), the transmitter includes a non-stop wave (CW) laser as an optical strength supply and is modulated via way of means of a PRBS sample generator that produces a binary facts sequence [11]. The modulated enter sign then propagates thru the FBG and displays a sign with the identical wavelength because the Bragg wavelength λB.

Bragg wavelength may be calculated via way of means of equation[14].

$$\lambda B = 2n\Lambda \qquad (1)$$

Where n is the refractive index of the silica, which is 1.45, is the period or step of the grating. The system is simulated with a single-mode fiber[15]

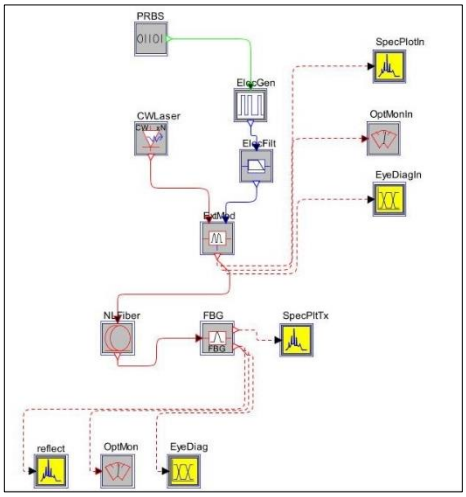

Figure 1: A single FBG sensor hydrophone system

In reality, the system also includes a circulator to circulate the reflected signal to the spectrum analyzer. As shows in figure (2) in reality, the system also includes a circulator to circulate the reflected signal to the spectrum analyzer.

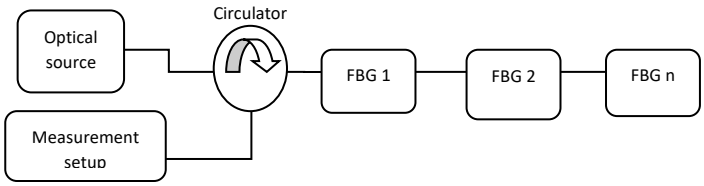

Figure 2: Real hydrophone system.

The very last gadget layout changed into organized with arrays of fiber Bragg gratings (FBGs)[16]. There is a complete of 5 FBGs withinside the gadget, and every FBG is a part of a distance of fifty m due to the fact the simulation is for small sensors[17,18] The general distance of the gadget is three hundred m, which may be seemed as short-variety telemetry. Its shape is proven in Figure (3)[17].

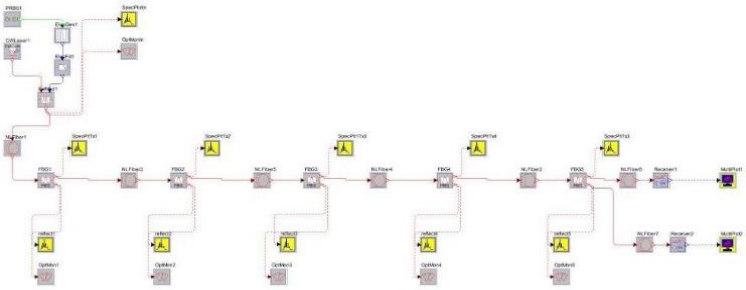

Figure 3: An array of FBGs in sensor hydrophone system.

The system uses wavelength division multiplexing (WDM) to return a reflected signal. Bragg wavelength has been reflected in the measurement setup. Since each FBG has its own Bragg wavelength, WDM technology can be applied by assigning a different Bragg wavelength to each FBG[18]. As shows in figure (4) the wavelength range of each FBG that used to design the system.

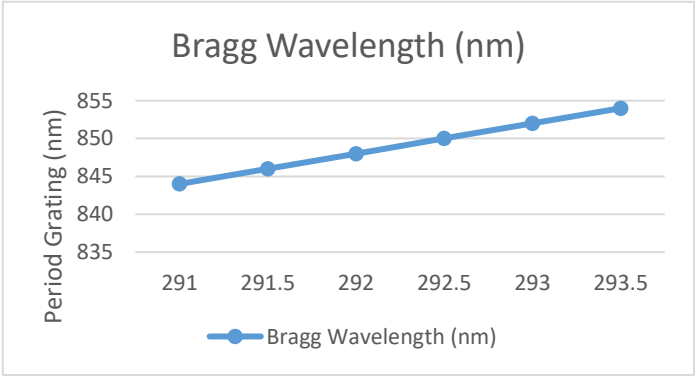

Figure 4: Bragg wavelengths for each FBG.

The system is designed to detect seismic changes when detecting changes in seafloor loads and temperatures. Due to the temperature change of the fiber, the Bragg wavelength λB shifts due to thermal expansion, and the grating interval Λ changes as a function of temperature. The wavelength shifts at the center of the FBG due to temperature changes $\Delta\lambda_{BT}$ can be obtained from Eq. (2)[19]

$$\Delta\lambda_{BT} = 2\left(\Lambda\frac{\partial n_{eff}}{\partial T} + n_{eff}\frac{\partial\Lambda}{\partial T}\right)\Delta T \quad (2)$$

where $\Delta T = (T - T_{\circ})$, $T(^{\circ}C)$ is the heating temperature and $T_0(^{\circ}C)$ is the reference temperature. The thermal expansion equation can be rewritten as (3)[19]:

$$\Delta\lambda BT = \lambda o\,(\alpha\Lambda + \alpha n)\,\Delta T \quad (3)$$

Where αΛ is the thermal expansion coefficient for the fiber and equals 0.55x10-6 for the silica. The quantity αn represents the thermo-optical coefficient of for quartz cores doped with Germania, which is approximately equal to 8.3 x 10 -6 for FBG. λo is the center wavelength of the fiber bragg grating at T_o When the fiber is stretched, the Bragg wavelength changes as the grating period changes, so the strain affects the sensor as well. The dilation changes the Bragg wavelength by expanding or compressing the grating and changing the effective refractive index. The shift ΔλBS of the central wavelength of the Bragg grating due to the stress change is deduced from the following equation[19]:

$$\Delta\lambda_{BS} = 2\left(\Lambda\frac{\partial n_{eff}}{\partial L} + n_{eff}\frac{\partial\Lambda}{\partial L}\right)\Delta L \quad (4)$$

Where ΔL is the change in length of the fiber Bragg grating due to strain. This shift, $\Delta\lambda_{BS}$ due to an applied strain on the FBG can be expressed by[19]:

$$\Delta\lambda_{BS} = \lambda_0(1 - P_e).\Delta\varepsilon_z \quad (5)$$

with ε_z is the strain in z-direction and P_e the effective strain-optic constant defined as

$$P_e = \frac{n^2{}_{eff}}{2}\{P_{12} - v(P_{11} - P_{12})\} \quad (6)$$

Where P_{11} and P_{12} are components of the strain-optic sensor and v is Poisson's ratio. For a typical silica Fiber$P_{11} = 0.113$, $P_{12} = 0.252$, $v = 0.16$, and n_{eff} = 1.45. Using these values, the effective strain optic constant is found as Pe = 0.29. Figure (5) below shows an overview of the practical sensing method of the FBG, highlighting the shift of the light with applied strain.

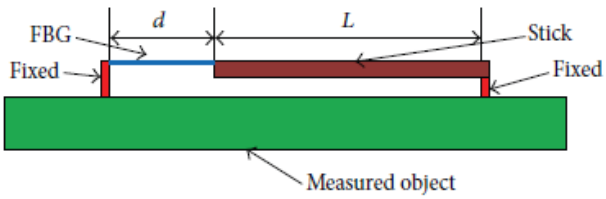

Figure 5: Practical sensing method of the FBG[20].

All of the above formulas have already been applied to Optisim software. The only task I had to do reresnts changing the parameters of the system. For example, the temperature and grid period have been changed to reflect the actual strain changes. Obviously, the strain could not be physically achieved within the simulation.

2.1 Input Wavelengths

This section describes the input wavelengths used by the system. The wavelength commonly used for each device is the lowest damping window. Optical fiber transmitters and receivers are generally classified as AGRIITEINIG than one of the three frequencies. As shown in FIG. 4, it is found that these frequencies have minimum attenuation over the full frequency band. 5[21]. The minimum damping area is called a window. Common wavelengths used in the industry are 850 nm, 1300 nm, and 1550 nm.

850nm technology is readily available at the lowest cost which considerd the first band used for fiber optic communications in the 1970s and early 1980s[22]. This was due to a local dip in the attenuation profile of the "optical fiber of the time" attractive, but (mostly) people in this band can use cheap light sources and detectors. Although this does not have minimal attenuation or unpredictability, it works best when combined with the least expensive (and most effective) parts. GaAs for the transmitter and silicon for the detector.

This window enables cost-effective short-range connections or local area networks over low or medium bitrate multimode fibers. There is a new application for high bit rate (Gbps and above) short range links that use VCSEL laser diodes on multimode fibers[23].

However, fiber optic cables withinside the 850nm band have better attenuation than the 1300nm band and decrease bandwidth. This band round 1310 nm turned into used withinside the mid-1980s. This band is appealing nowadays due to the fact single-mode fibers don't have any fiber dispersion. Light reassets and detectors on this band are extra pricey than the fast wave band (850 nm). This is the bandwidth that maximum long-variety verbal exchange structures perform nowadays.

1300m receivers and transmitters are extra pricey, however have much less loss and are encouraged for long-distance coverage. The loss is generally much less than 0.five dB in line with kilometer. 850nm generation is generally utilized in multimode applications, even as 1300nm generation is used withinside the single-mode or multimode operation.

1550 nm is suitable for long-distance communication applications with a loss of approximately 0.2 dB per kilometer. This band has the lowest loss available on current fibers. Optical amplifiers operating in this band are also available. However, it is difficult (expensive) to create a light source and detector that works here. Standard fibers also propagate signals in this band. thus, it meets the absolute minimum attenuation, but due to wavelength dispersion issues, more expensive components (monochromatic laser DFB diodes, and finally dispersion compensators) are required. Today, it is primarily used for long-

distance connections over single-mode fiber (ground or seafloor) over 100 km, with bit rates of several gigabits per second. At this wavelength, optical amplification is used and large-scale wavelength division multiplexing is applied. In the late 1990s, almost all new communication systems could operate on this volume.

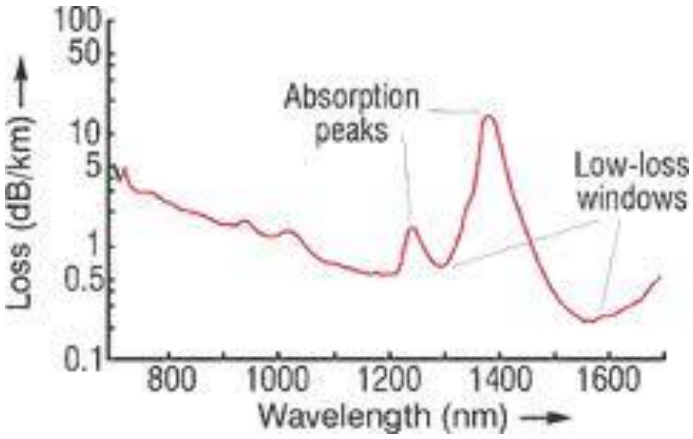

Figure 6: Lowest attenuation window[21].

3. Results and Analysis

The simulation is performed by changing the input wavelengths to 850 nm, 900 nm, 1000 nm, 1300 nm, 1400 nm, and 1550 nm. The measured power is taken from the last FBG. The results obtained are as follows.

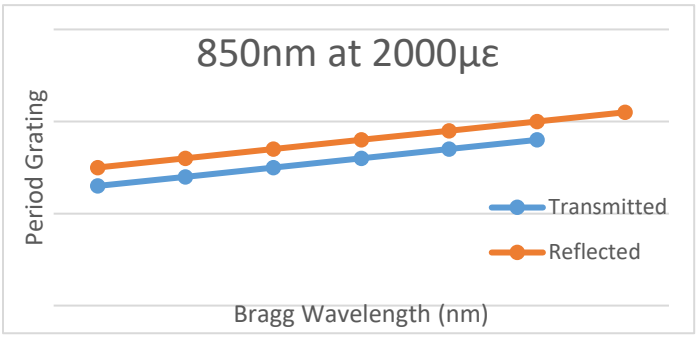

Figure 7: Reflected wavelength at 2000με.

Fig.7. shows an example of reflected Bragg wavelength taken at 850nm as input wavelength and at 2000με. It turns out that due to expansion and temperature changes, the reflected wavelength has changed.

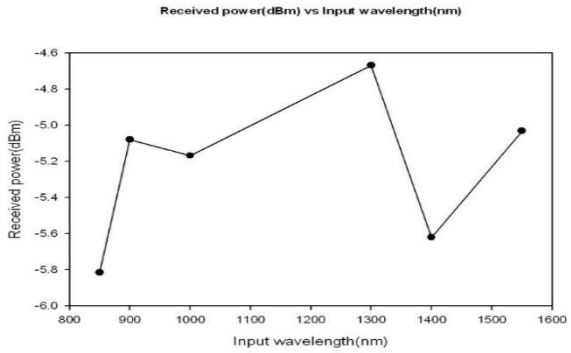

Figure 7: Received power measured.

This shows that the 1300 nm and 1550 nm input wavelengths provide the best system performance for power attenuation and the 850 nm inputs provide the lowest performance. This result is in line with the expected result as 1300nm and 1550nm are in the lowest attenuation window. In addition, there is no fiber dispersion in single-mode fibers with a wavelength of 1300 nm.

3.1 Bragg Wavelengths setting

Optical communication links are very powerful because they can simultaneously carry different wavelength ranges from 1300 to 1600 nm on a single fiber. This technology's ability to combine multiple wavelengths on the same fiber is known as wavelength division multiplexing (WDM). Conceptually, the WDM scheme is similar to frequency division multiplexing (FDM) used in satellite radio and satellite systems. Like FDM, WDM requires appropriate wavelength (or optical frequency) spacing to avoid interference between channels.

WDM systems rely on the ability of fiber optic cables to carry many different wavelengths without interfering with each other. Each wavelength represents the optical channel of a fiber optic cable. Several optical schemes are available to combine the individual channels of a fiber optic cable and connect them to the network at the appropriate points. WDM technology has developed to reduce the wavelength spacing of channels to a few nanometers, resulting in a high-density division multiplexing (DWDM) system.

Fiber optic hydrophones, including fiber bragg gratings, used wavelength division multiplexing because the system consists of multiple sensors that are FBGs. The concept of FBG is to reflect and return the same wavelength as the Bragg wavelength λB described at the beginning. Therefore, in this system, five reflected signals are sent through the fiber to the spectrum analyzer, as shown in Figure 9.

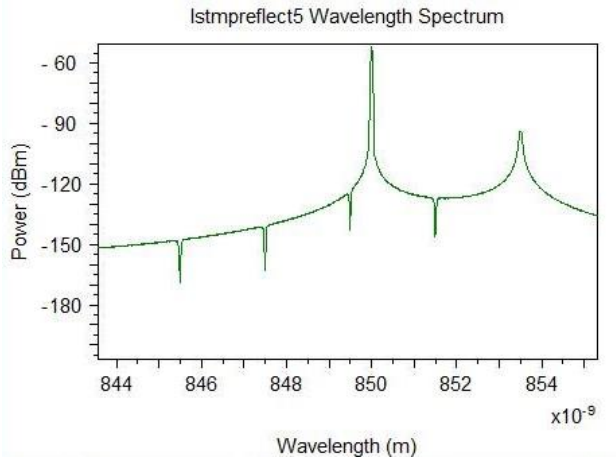

Figure 8: Reflected wavelengths taken from the last FBG.

Bragg wavelength is established by using equation (1). This is $\lambda B = 2n\Lambda$.

In reality, these wavelengths were written when the FBG was created. These wavelengths do not shift unless strain or temperature changes are applied. Tables 1-6 show Bragg wavelengths and grating periods that vary over the input wavelength range of 850 to 1550 nm.

Table 1: Bragg wavelength for 850nm input wavelength.

Fiber Bragg Grating	Bragg Wavelength(nm)	Period grating(nm)
1	845.5	291.55
2	847.5	292.24
3	849.5	292.93
4	851.5	293.62
5	853.5	294.31

Table 2: Bragg wavelength for 900nm input wavelength.

Fiber Bragg Grating	Bragg Wavelength(nm)	Period grating(nm)
1	892	307.59
2	894	308.28
3	896	308.97
4	904	311.72
5	906	312.41

Table 3: Bragg wavelength for 1000nm input wavelength.

Fiber Bragg Grating	Bragg Wavelength(nm)	Period grating(nm)
1	996	343.45
2	998	344.14
3	1002	345.52
4	1004	346.21
5	1006	346.90

Table 4: Bragg wavelength for 1300nm input wavelength.

Fiber Bragg Grating	Bragg Wavelength(nm)	Period grating(nm)
1	1294	446.21
2	1296	446.90
3	1302	448.97
4	1304	449.66
5	1306	450.34

Table 5: Bragg wavelength for 1400nm input wavelength.

Fiber Bragg Grating	Bragg Wavelength(nm)	Period grating(nm)
1	1394	480.69
2	1396	481.38
3	1402	483.45
4	1404	484.14
5	1406	484.83

Table 6: Bragg wavelength for 1550nm input wavelength.

Fiber Bragg Grating	Bragg Wavelength(nm)	Period grating(nm)
1	1544	532.41
2	1546	533.10
3	1552	535.17
4	1554	535.86
5	1556	536.55

3.2 Strain Calibration

As shown in Table 7, the flexibility of the OptSim parameters is limited. Therefore, it is necessary to change the grating cycle to change the strain. However, it is acceptable to change the FBG temperature parameters. Obviously, physically changing the load is not practical since the software does not have strain function FBG sensor works at the precept of wavelength shift. According to coupled-mode theory, Bragg wavelength relies upon the physical parameters of fiber which might be the grating period and powerful refractive index. Shift withinside the wavelength of the reflected spectrum both to the left or right of the central wavelength is prompted best if both the period of gratings or powerful refractive index of FBG is modified by the parameter to be measured, which includes temperature, strain, humidity, pressure, etc. According to Bragg condition, wavelength extrade may be found, that be indicative of the quantity of external perturbation implemented on FBG

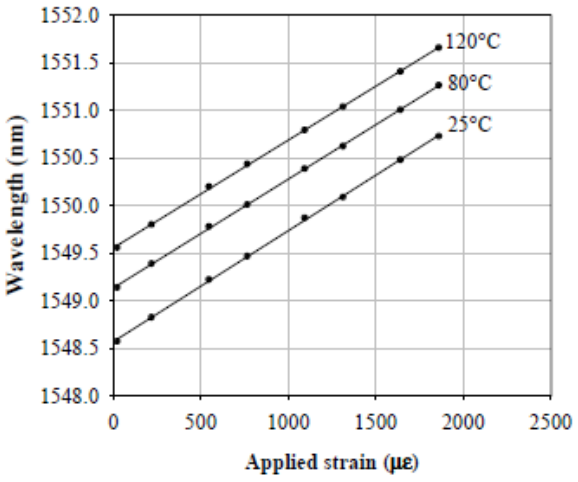

Figure 10: Wavelength change as a function of applied strain for the FBG at three different temperatures[24].

Table 7: FBG default parameters setting.

Name	Type	Default	Range	Units
Period	double	5.35355e-7	[0,1e32]	m
Length	double	1.0e-2	[0,1e32]	m
Modulation Depth	double	1.0e-4	[-1e32,1e32]	none
Refractive index	double	1.45	[0,1e32]	none
Linear Chirp	double	0	[-1e32,1e32]	nm
Apodisation Patern	enumerated	Uniform Grating	Uniform Grating cosine raised Simusoid, Tanh, blackman	
Apodistation coef	double	0	[-1e32,1e32]	none
Temperature	double	20.0	[0,1e32]	C

Calibration is performed by checking the results of actual work, as it is shown in Figure 9[24]. Y is the wavelength in nm and X is the applied stress in με. This result is used in the OptSim strain simulation. Therefore, it will be imported from the actual results.

The graph in Figure 9 is used as a generic reference due to the software does not have strain function. These practical results are converted and summarized in Table 8. This was to determine the grating period changes for applied strains.

Table 8: Grating period, Λ by applied strain.

X-axes Strain ($\mu\epsilon$)	Y-axes Wavelength (nm)	$\Lambda(nm)=\frac{\lambda}{2neff}$
0	1548.50	533.97
500	1549.03	534.15
1000	1549.55	534.33
1500	1550.08	534.51
2000	1550.60	534.69

From Table 8, it is found that the grating period will increase by addition of 0.18 nm for every 500 με increase in strain. This value is important for the applied strain in different temperature conditions. The initial FBG wavelength h is set as a reference at ambient temperature (20°C). Table 9 presents the Bragg wavelength shift measurements due to applied strain and temperature for each of the 5 gratings used in the set-up:

FBG_1 = 1540 nm FBG_2 = 1543 nm FBG_3 = 1545 nm
FBG_4 = 1554 nm FBG_5 = 1556 nm

For many cases related to the discrimination between two or more parameters such as strain and temperature, several conditions such as in the above data, are important. By applying the first task recommendation, each FBG is assigned to a specific value of wavelength so that no overlap case will occur while changing the strain and temperature parameter. Every increasing strain and temperature values will increase the Bragg wavelength shift. From the figures, the researchers plot the gradient of the line-of-best (LOBF) for both graphs using sigma-plot software. By obtaining the gradient for each graph, the sensitivity is estimated. For any measurement of strain or temperature, the sensitivity of the temperature change is usually about ten times that of the strain change. Figure 10 below shows shifts in the FBG wavelength with temperature for a different strain applied.

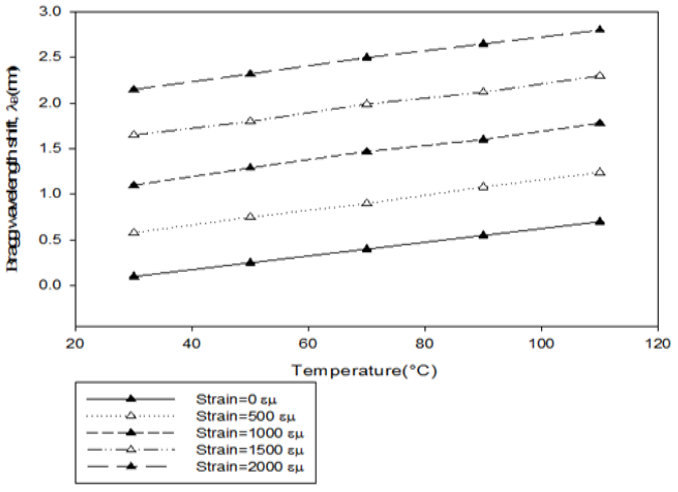

Figure 10: Shifts in the FBG wavelength with temperature for a different strain applied.

Table 9: Bragg wavelength shifts measured due to applied strain.

BG at 20°C(nm)	Temperature (°C)	Strain=0μ		Strain=500μ		Strain=1000μ		Strain=1500μ		Strain=2000μ	
		$\lambda_B(nm)$	$\Delta\lambda_B(nm)$	$\lambda_B(nm)$	$\Delta\lambda_B(nm)$	$\lambda_B(nm)$	$\Delta\lambda_B(nm)$	$\lambda_B(nm)$	$\Delta\lambda_B(nm)$	$\lambda_B(nm)$	$\Delta\lambda_B(nm)$
1540	30	1540.1	0.1	1540.58	0.58	1541.1	1.1	1541.65	1.65	1542.15	2.15
1545	50	1543.25	0.25	1543.75	0.75	1544.29	1.29	1544.8	1.8	1545.32	2.32
1556	70	1545.4	0.4	1545.9	0.9	1546.47	1.47	1546.99	1.99	1547.5	2.5
1543	90	1554.55	0.55	1555.08	1.08	1555.6	1.6	1556.12	2.12	1556.65	2.65
1554	110	1556.7	0.7	1557.24	1.24	1557.78	1.78	1558.3	2.3	1558.8	2.8

Figure 12 below shows shifts in the FBG wavelength with strain for a different temperature applied:

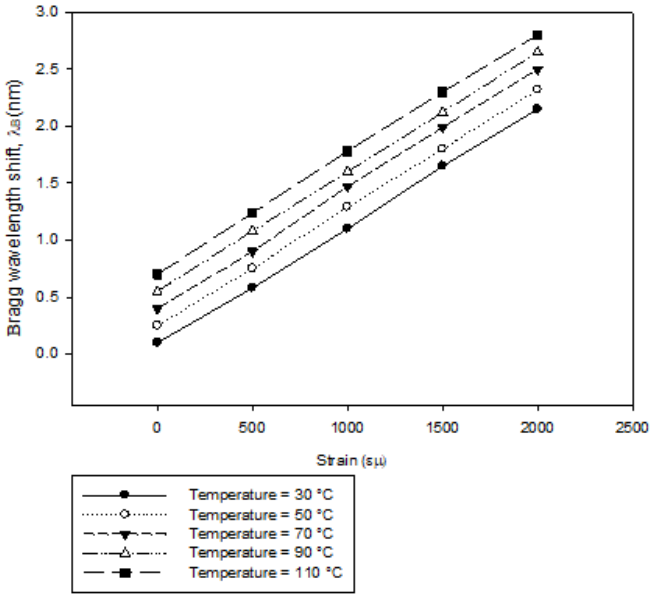

Figure 12: Shifts in the FBG wavelength with strain for a different temperature applied.

By assuming the distribution line in the above figures having the same gradient m, the sensitivity of the temperature and strain can be obtained:

$$\text{linear equation, } y = mx + c$$

$$\text{average sensitivity of the strain} \approx 1.046\ \text{pm}/\mu\varepsilon$$

$$\text{average sensitivity of the temperature} \approx 8.07\ \text{pm}/^{\circ}\text{C}$$

Now it can be discriminated between the two parameter changes due to strain and temperature, at any position in the FBG array sensor. It is worthly mentioned that the average sensitivity value of the temperature should be ten times that of the strain value. There are several reasons for the slightly inaccurate values obtained. These factors has been identified and understood. Below is a list of probable reasons: -

a) Mistaken readings of graphs.

b) Strain assumptions based on practical values.

c) Task fully done by software simulation.

4. Conclusion

In this paper, a detailed simulation study of a seismic sensing system with a fiber optic hydrophone will be performed. The system consists of a fiber optic Bragg grating (FBG), which uses a variety of light source wavelengths. Two main parameters affect FBG Load and temperature. In this study, we tested six input source wavelengths. These are 850 nm, 900 nm, 1000 nm, 1300 nm, 1400 nm and 1550 nm.

By combining the results, designers can optimize the performance of future analog fiber-optic hydrophones. The 1300 nm wavelength range has been proven to deliver the best performance for this type of fiber optic underwater sound system due to the 1300 nm Bragg wavelength is more sensitive than 1400 nm and 1550 nm because the 1300 nm wavelength has greater attenuation than the 1550 nm wavelength. The wavelength used affects the modes of wave propagation as a function of the refractive index of FBG.

Conflict of interests

None.

References

[1] G. A. Cranch, P. J. Nash, and C. K. Kirkendall, "Large-scale remotely interrogated arrays of fiber-optic interferometric sensors for underwater acoustic applications," *IEEE Sens. J.*, vol. 3, no. 1, pp. 19–30, 2003.

[2] O. Mahran, T. A. Hamdallah, M. H. Aly, and A. E. El-Samahy, "Compensation of Bragg wavelength shift under sea level using a nonlinear FBG," *Natl. Radio Sci. Conf. NRSC, Proc.*, no. May 2014, 2006.

[3] W. W. Morey, G. Meltz, and W. H. Glenn, "Fiber Optic Bragg Grating Sensors," *Fiber Opt. Laser Sensors VII*, vol. 1169, no. February 1990, p. 98, 1990.

[4] K. R. Tariq, R. A. Johni, and D. I. Forsyth, "Comparative Accuracies of Fiber Bragg Grating Sensing Systems for Temperature Measurement," *Res. J. Appl. Sci. Eng. Technol.*, vol. 16, no. 5, pp. 212–220, 2019.

[5] H. Mikada and K. Asakawa, "Development of japanese scientific cable technology," *Ocean. 2008*, pp. 1–4, 2008.

[6] W. Zhang, F. Li, Y. Liu, and H. Xiao, "FBG hydrophone: Theory and experiment," *2008 1st Asia-Pacific Opt. Fiber Sensors Conf. APOS 2008*, vol. 6, no. 4, pp. 2008–2011, 2008.

[7] M. Berrada, R. A. Secco, W. Yong, and J. A. H. Littleton, "Electrical Resistivity Measurements of Fe-Si With Implications for the Early Lunar Dynamo," *J. Geophys. Res. Planets*, vol. 125, no. 7, 2020.

[8] H. Dobb *et al.*, "Continuous wave ultraviolet light-induced fiber Bragg gratings in few- and single-mode microstructured polymer optical fibers," *Opt. Lett.*, vol. 161, no. 8, pp. 417–482, 2003.

[9] F. D. Mahad, A. S. M. Supa'At, S. M. Idrus, and D. Forsyth, "Modeling of semiconductor optical amplifier gain characteristics for amplification and switching," *AIP Conf. Proc.*, vol. 1345, no. April 2017, pp. 217–220, 2011.

[10] K. Tariq, D. I. Forsyth, and R. A. Johni, "Further Investigation of Intensity Noise Reduction on an Incoherent Light Source using a Gain Saturated Semiconductor Optical Amplifier in a Spectrum-sliced Channel at 2.5 Gb\\s," *Res. J. Appl. Sci. Eng. Technol.*, vol. 12, no. 7, pp. 700–705, 2016.

[11] Zhongjie Ren, Ke Cui, Jianxin Li, Rihong Zhu, Qing He, Hailing Wang, Shaokun Deng, and Wenjun Peng, 'High-quality hybrid TDM/DWDM-based fiber optic sensor array with extremely low crosstalk based on wavelength-cross-combination method,' Opt. Express 25, 2," vol. 28885, p. 28885, 2017.

[12] G. Allwood, G. Wild, and S. Hinckley, "Optical Fiber Sensors in Physical Intrusion Detection Systems: A Review," *IEEE Sens. J.*, vol. 16, no. 14, pp. 5497–5509, 2016.

[13] X. Qiao, Z. Shao, W. Bao, and Q. Rong, "Fiber bragg grating sensors for the oil industry," *Sensors (Switzerland)*, vol. 17, no. 3, 2017.

[14] J. Rutqvist, H. Liu, D .W. Vasco, "Fiber optic distributed sensing technology for real-time monitoring water jet tests: Implications for wellbore integrity diagnostics," vol. 3, no. 2, p. 6, 2021.

[15] D. Tosi, "Improved KLT Algorithm for High-Precision Wavelength Tracking of Optical Fiber Bragg Grating Sensors," *J. Sensors*, vol. 2017, 2017.

[16] A. Lamberti, S. Vanlanduit, B. De Pauw, and F. Berghmans, "A novel fast phase correlation algorithm for peak wavelength detection of fiber Bragg grating sensors," *Opt. Express*, vol. 22, no. 6, p. 7099, 2014.

[17] S. Liu, B. Liu, and W. Yang, "Highly sensitive mass detection based on nonlinear sum-sideband in a dispersive optomechanical system," Opt. Express 27, 3909-3919 ,2019.

[18] J. Dai, M. Yang, Y. Chen, K. Cao, H. Liao, and P. Zhang, "Side-polished fiber Bragg grating hydrogen sensor with WO_3-Pd composite film as sensing materials," *Opt. Express*, vol. 19, no. 7, p. 6141, 2011.

[19] M.H. Aly, H. Fayed, "Compensting Bragg Wavelength Drift due to Temperature and Pressure by Applying an Artificial strain " December , 2004.

[20] R. F. Syahputra, Saktioto, R. Meri, Syamsudhuha, and Okfalisa, "Profile of single mode fiber coupler combining with Bragg grating," *Telkomnika (Telecommunication Comput. Electron. Control.*, vol. 15, no. 3, pp. 1103–1107, 2017.

[21] C. Mounia, A. Otman, A. A. Badiaa, C. Fahd, A. A. Vazquez, and E. Y. Mounir, "Gain flatness and noise figure optimization of C-Band EDFA in 16-channels WDM System using FBG and GFF," *Int. J. Electr. Comput. Eng.*, vol. 7, no. 1, pp. 289–298, 2017.

[22] A. Ikhlef,R. Hedara,M. Chikh-bled, "Uniform Fiber Bragg grating modeling and simulation used matrix transfer method ," *Lean Lead.*, vol. 9, no. 1, pp. 120–131, 2012.

[23] J.-Y. Huang *et al.*, "FBGs written in specialty fiber for high pressure/high temperature measurement," *Opt. Express*, vol. 25, no. 15, p. 17936, 2017.

[24] T.B. Nguyen, "Determining Rare E a r t h Dopant Concentrations in Optical Fibres and Waveguides," 2004.